Volume 3 | Number 8 | August 2019

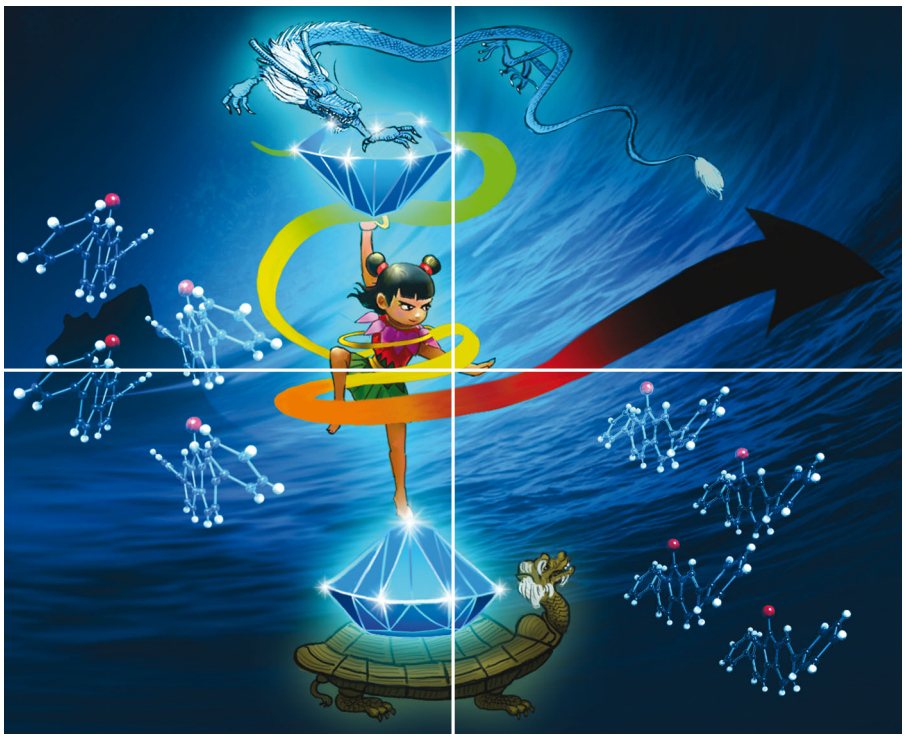

MATERIALS CHEMISTRY

FRONTIERS

CCS 中国化学会 CHINESE CHEMICAL SOCIETY

ICCAS 1956

ROYAL SOCIETY OF CHEMISTRY | Celebrating IYPT 2019

rsc.li/frontiers-materials

MATERIALS CHEMISTRY
FRONTIERS

RESEARCH ARTICLE

View Article Online
View Journal | View Issue

Cite this: *Mater. Chem. Front.*, 2019, **3**, 1510

Drastic photoluminescence modulation of an organic molecular crystal with high pressure†

Junjie Guan,[ab] Chunfang Zhang,[c] Dexiang Gao,[b] Xingyu Tang,[b] Xiao Dong,[d] Xiaohuan Lin,[b] Yajie Wang,[b] Xinxin Wang,[b] Lin Wang,[b] Hyun Hwi Lee,[e] Jialiang Xu,*[af] Haiyan Zheng,*[b] Kuo Li[b] and Ho-kwang Mao[b]

Received 7th February 2019,
Accepted 5th April 2019

DOI: 10.1039/c9qm00082h

rsc.li/frontiers-materials

Pressure is an effective method to modulate the optical properties of organic solid-state light-emitting materials through enhancing intermolecular interactions and/or generating new polymorphs. Herein, we find that the organic molecular crystal of diphenylfluorenone (DPFO) undergoes a large-scale and continuous redshift of the UV-vis absorption and photoluminescence (PL) spectra under high pressure, across the entire visible light region. Remarkably, a redshift of about 300 nm was observed for its PL peak at 13.32 GPa, from greenish-yellow to the near-infrared (NIR) region. The *in situ* high-pressure IR spectra and synchrotron X-ray diffraction (XRD) analyses suggest a phase transition from the α- to the γ-phase (newly identified) at around 3 GPa, accompanied by the phenyl unit in DPFO converting from perpendicular to parallel packing. Theoretical calculations show that the enhanced π···π interactions and the overlap of the molecular orbitals in the γ-phase are responsible for such a tremendous redshift in the PL spectra. Our work highlights the large redshift phenomenon in the DPFO system under high pressure, which may have potential photonic device applications. Furthermore, this work reveals the clear structure-property relation, providing deep insight into the tailoring of the optical characteristics of molecular materials.

Introduction

Organic solid-state light-emitting materials, whose luminescence can be tuned by external stimuli, have attracted considerable research interest for their potential applications in optical storage, sensors, multi-colour displays and security papers.[1–5] The optical properties of these materials are not only related to the photoactivity of the molecular building blocks, but also to the packing modes of these luminescent molecules.[6–8] By using traditional methods such as solution-processed self-assembly[9,10] or the co-crystal strategy,[11] different crystal structures can be obtained from the same molecules, *i.e.*, polymorphs, which is an effective method to tailor their luminescent properties.[12,13] Recently, the fast-developed high-pressure technologies have provided an effective method to generate new polymorphs, and thus, to modulate the luminescent properties by changing the molecular arrangements.[14–16] Due to enhanced intermolecular interactions or restricted molecular vibrations under high pressure, redshift and/or increased emission intensity have been observed under such extreme conditions.[17,18] For example, by compressing the anthracene derivative, a redshift of 100 nm was observed due to the enhanced intermolecular π···π interactions.[19] Zou *et al.* reported that pressure could induce the tautomerization of spiropyran, resulting in a redshift of over 190 nm of the luminescence.[20,21] The increased N–H···π interaction and the restriction of the N–H stretching vibration were responsible for the pressure-induced emission enhancement (PIEE) phenomenon detected in the carbazole system.[22] In this context, discovering and designing new pressure responsive systems and understanding the relationship between their photophysical properties and packing modes is extremely important for advancing their applications in diverse fields, such as optical pressure-sensing devices.

Diphenylfluorenone (DPFO), featuring a typical supramolecular structure with molecular chains held together by hydrogen bonds and C–H···π interactions, exhibits brilliant nonlinear optical properties.[23] It can readily be grown into large crystals for THz generators and detectors through simple

[a] *School of Chemical Engineering and Technology, Tianjin University, Tianjin 300350, China. E-mail: jialiang.xu@tju.edu.cn*
[b] *Center for High Pressure Science and Technology Advanced Research (HPSTAR), Beijing 100094, China. E-mail: zhenghy@hpstar.ac.cn*
[c] *College of Chemistry and Environmental Science, Hebei University, No. 180 Wusidong Road, Baoding 071002, Hebei, P. R. China*
[d] *Key Laboratory of Weak-Light Nonlinear Photonics, School of Physics, Nankai University, Tianjin 300071, China*
[e] *Pohang Accelerator Laboratory, POSTECH, Pohang 790-784, Republic of Korea*
[f] *School of Materials Science and Engineering, Nankai University, Tianjin 300350, China. E-mail: jialiang.xu@nankai.edu.cn*

† Electronic supplementary information (ESI) available. See DOI: 10.1039/c9qm00082h

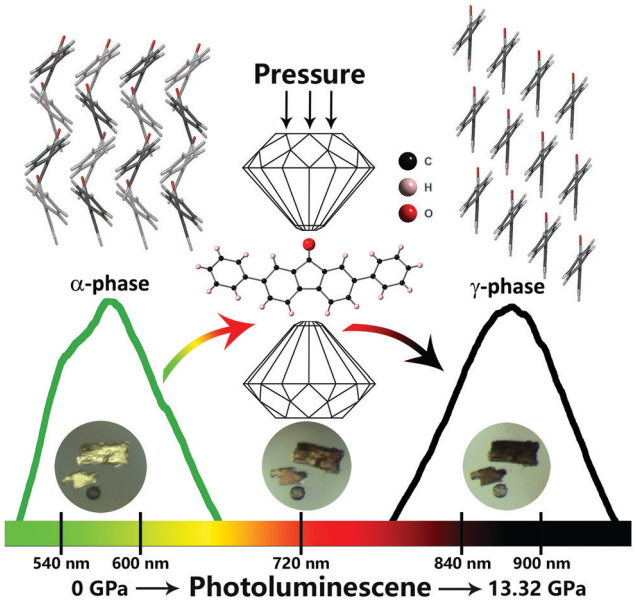

Scheme 1 The relationship between the optical properties and the crystal structures of the DPFO crystals under high pressure.

solution processes at ambient conditions.[24] The limited rotation of DPFO upon aggregation results in a dramatic enhancement of the linear optical emission when forming self-assemblies.[23,25] By controlling the operation conditions such as temperature and solvents, DPFO can form two different polymorphs, namely the α-phase (orthorhombic, space group $Ccm2_1$) and the β-phase (orthorhombic, space group *Pbca*), which show very different linear and nonlinear optical responses.[9] In this work, we applied high pressure to tailor the molecular configuration and packing modes, and therefore, modulate the optical properties of DPFO-based molecular crystals. By compressing the DPFO crystals, a colour change from yellow to dark red and a drastic and consecutive luminescence shift (~300 nm) was observed upon the application of high pressure (>10 GPa) (Scheme 1). The maximum emission wavelength reached 875 nm, which was in the NIR region. *In situ* IR and synchrotron X-ray diffraction (XRD) measurements suggest the generation of a new phase (referred to as the γ-phase) at high pressure above 3 GPa. In this new phase, the phenyl rings turned from perpendicular packing to parallel packing, which enhanced the π···π interactions. Theoretical calculations reveal that the formation of the strong face-to-face stacking of the DPFO molecules results in orbital overlap between neighboring molecules, which may be responsible for the massive redshift of the UV-vis absorption and the corresponding photoluminescence spectra. Our studies highlight pressure as an effective technique to fine-tune the optical properties of the molecular crystalline materials by generating new polymorphs. The closed packing structure under high pressure will lead to a large-scale redshift which is very difficult to achieve by other stimuli. The clear relationship between the high-pressure crystal structure and corresponding optical properties indicated here will contribute to understanding the conformation, structure and luminescence characteristics of the fluorophore.

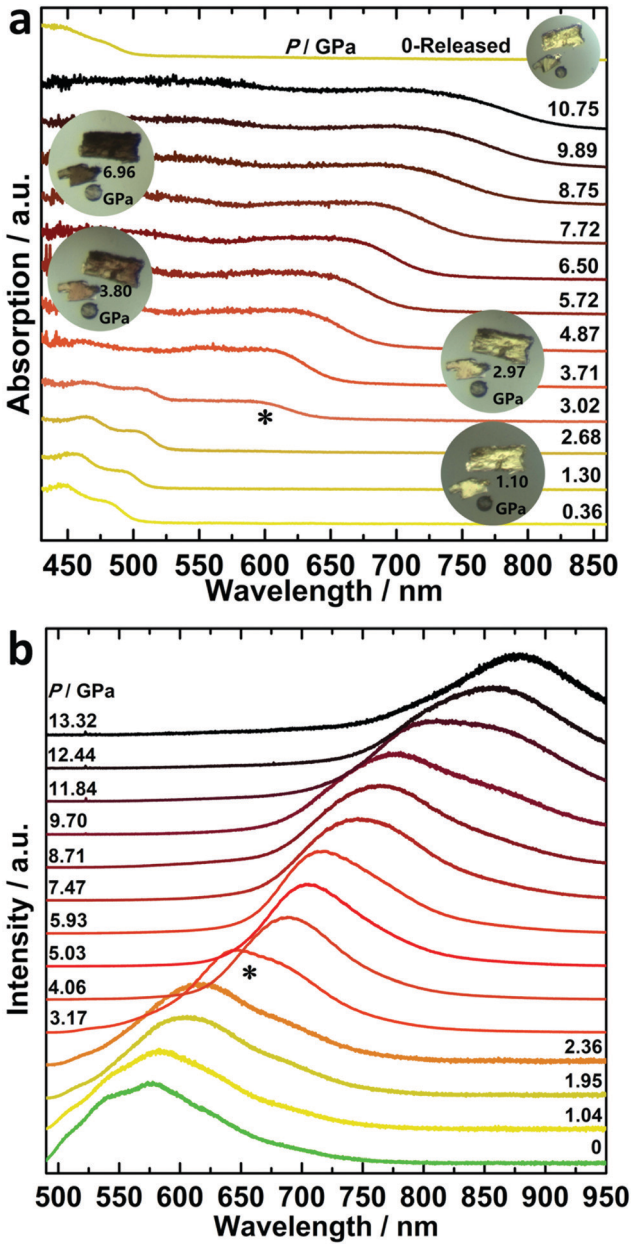

Fig. 1 The *in situ* (a) UV-vis absorption and (b) photoluminescence (PL) spectra of DPFO under high pressure (asterisk in the UV-vis spectra represents the observed new peak and that in the PL spectra represents the jump of red-shift). The "0-released" in the UV-vis absorption spectra corresponds to the spectrum of DPFO released from 10.75 GPa. The insets in (a) are the optical images obtained from the microscope under compression (the black ball is a ruby ball for pressure measurement).

Results and discussion

In situ high-pressure UV-vis absorption and photoluminescence spectra

Pressure is a straightforward and effective way to regulate the optical properties of materials. As shown in the insets of Fig. 1a, the colour of the DPFO crystal is yellow with good transparency at 1.10 GPa. When compressed, it turned pale red at 2.97 GPa and finally to dark red at 6.96 GPa. Correspondingly, the UV-vis

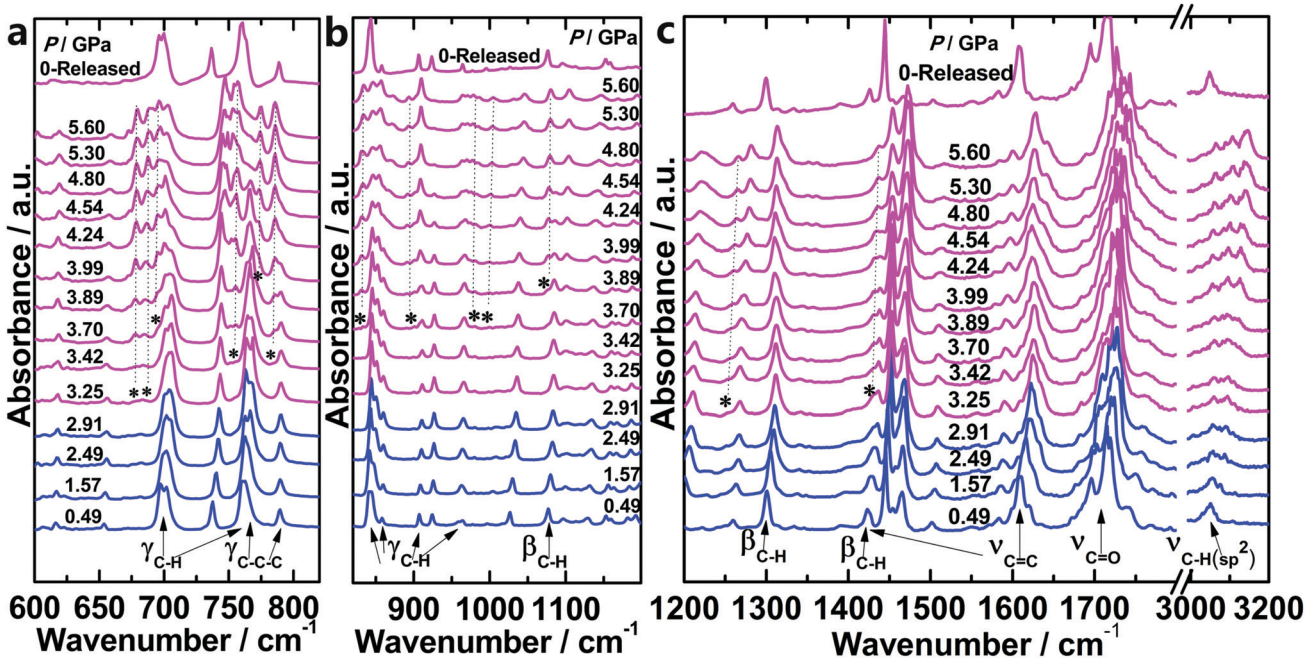

Fig. 2 The IR spectra of the DPFO crystal with increasing pressure from 0.49 GPa to 5.60 GPa and decompressed from 5.60 GPa (0-released). The new peaks are indicated by asterisks. (a) 600–820 cm^{-1}, (b) 820–1200 cm^{-1} and (c) 1200–3200 cm^{-1}.

absorption spectra showed obvious redshift upon increasing pressure. At 0.36 GPa, the main absorption peak was around 475 nm, which redshifted upon compression. At 3.02 GPa, a new broad peak (asterisk in Fig. 1a) centered at 575 nm was observed, which resulted in the colour change from yellow to red. Upon further compression, this peak became broader and shifted to the longer wavelength region continuously and finally crossed the entire visible light region at 10.75 GPa. Upon decompression to ambient pressure, the absorption spectra recovered to their original state, which provided evidence for the reversible variation. Selected photoluminescence (PL) spectra under high pressure are shown in Fig. 1b. At ambient pressure, the emission band was centered at 575 nm. This maximum luminescence peak (λ_{max}) gradually redshifted during compression. At 3.17 GPa, a sudden redshift jump was observed (asterisk in Fig. 1b), corresponding to the new absorption peak, as shown in the UV-vis absorption spectra. Eventually, the luminescence peak λ_{max} reached 875 nm at 13.31 GPa, in the near-infrared region. Such a large wavelength variation of 300 nm in the luminescence spectra is rarely achievable with other stimuli. Additionally, the intensity of the photoluminescence gradually decreased during compression up to 13.31 GPa (Fig. S1, ESI†). The enhancement of intermolecular interaction with increasing pressure is likely to be the reason for the redshift of the emission band and decrease in the PL intensity.[22] The new peak presented in the UV-vis absorption spectra and the sudden change in the PL spectra indicate a phase transition at around 3 GPa. Variations in the molecular conformation and aggregation under high pressure need to be investigated to understand this drastic change of optical properties in DPFO and its phase transition mechanism.

In situ high-pressure IR spectra

The *in situ* IR spectra were used to clarify this phase transition. The evolution of the IR spectra at various pressures is shown in Fig. 2. At ambient pressure, DPFO crystallized into an orthorhombic phase ($Ccm2_1$, the α phase) and the assignments of the DPFO IR modes are summarized in Table S1 (ESI†). By compressing the DPFO crystals from 0.49 to 2.91 GPa, most of the IR peaks revealed blueshift without the appearance of new peaks (Fig. 2a–c). Specifically, the C–H stretching vibration (ν_{C-H}) band at 3048 cm^{-1} blueshifted and split upon compression, which indicated the compression of the C–H bond and a change in the complex CH$\cdots\pi$ interaction under high pressure. At 3.25 GPa, three new IR peaks (675 cm^{-1}, 680 cm^{-1} and 1255 cm^{-1}) appeared in the low-frequency regions of the C–H out-of-plane bending vibration (γ_{C-H}) and C–H in-plane bending vibration (β_{C-H}), respectively. Meanwhile, the vibration at 1430 cm^{-1} corresponding to the C–H in-plane bending vibration (β_{C-H}) and C=C stretching ($\nu_{C=C}$) split. At 3.42 GPa, two new peaks appeared at 754 and 784 cm^{-1}, and their intensities were enhanced with increasing pressure. At 3.70 GPa and 3.89 GPa, a batch of new peaks was observed at 694, 832, 901, 981, 998 and 1076 cm^{-1}. In addition, the peaks of the α-phase at 697, 760, 788, 924, 1075, and 1422 cm^{-1} gradually degraded and were barely detectable above 3.99 GPa. Non-monotonic changes of the IR modes in the pressure range of 3.42–3.99 GPa were also observed (Fig. S2, ESI†). All of these changes indicate a phase transition starting at 3.25 GPa and finishing at 3.99 GPa, which is consistent with the evolution of the optical properties observed in the UV-vis and PL spectra. This new phase is quite different from the β phase obtained using the solvent method, as indicated by the

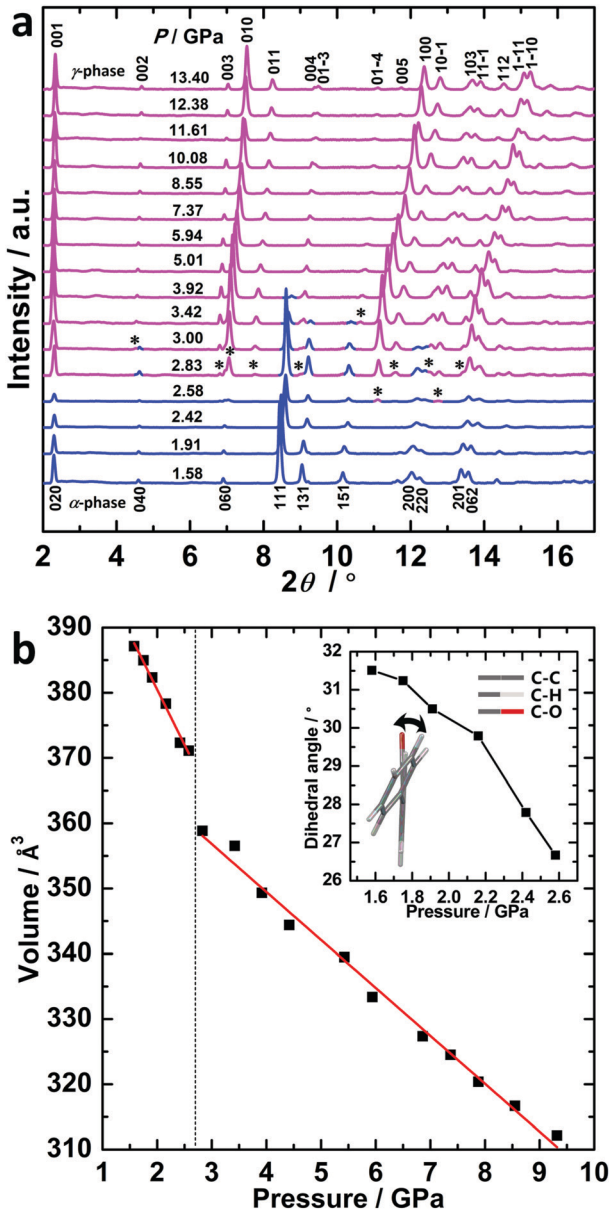

Fig. 3 (a) The synchrotron X-ray diffraction pattern of DPFO with increasing pressure (asterisks indicate the new diffraction peaks). (b) The variation of the averaged single molecular volume of DPFO at different pressures (the dotted line indicates the cell volume collapse) (inset: the variation of the dihedral angle before the phase transition).

X-ray diffraction described below.[9] Thus, this new phase hereafter is referred to as the γ-phase. The IR spectrum of DPFO recovered from 5.60 GPa is similar to the original state, which means that the phase transition from the α- to the γ-phase is fully reversible.

Synchrotron X-ray diffraction results and structural evolution

To obtain detailed information on the structural evolution and symmetry change of the DPFO crystals under high pressure, we performed synchrotron X-ray diffraction (XRD) experiments. The blue and pink peaks in Fig. 3a correspond to the α-phase and γ-phase, respectively. The patterns detected at 1.58 GPa fitted well to the α-phase by Rietveld refinement starting from the model reported in the literature (Fig. S3, ESI†).[23] The peaks of the α-phase with the $Ccm2_1$ group were clarified by Miller indices. The XRD profile changed significantly above 2.58 GPa. Two new diffraction peaks (100 and 11−1, marked by asterisks) emerged at around 11.1° and 12.8°, which indicated the onset of the phase transition. At 2.83 GPa, a batch of new diffraction peaks was observed and later indexed as 003, 010, 011, 004, 01−3, 10−1, 103 and 112. At 3.00 and 3.42 GPa, two new peaks (002 and 01−4) appeared at around 4.5° and 10.6°, respectively. Meanwhile, the peaks of the α-phase were hardly detectable above 3.92 GPa. All these indicate that the α- to γ-phase transition of DPFO began at 2.58 GPa and finished above 3.92 GPa. During the α-γ phase transition, the average single molecular volume collapsed from 371 Å^3 (at 2.58 GPa) to 358 Å^3 (at 2.83 GPa) (Fig. 3b), and the space group turned from $Ccm2_1$ to $P1$. The XRD pattern of the γ-phase was indexed *ab initio* (by software PowderX)[26] with a triclinic lattice of a = 3.4062(7) Å, b = 5.5126(15) Å, c = 17.434(6) Å, α = 98.34(3)°, β = 85.84(2)°, and γ = 84.218(14)°. The crystal structure was then solved using a simulated annealing method and Rietveld refinement (Fig. S4, ESI†). The solved structural model as shown in Fig. 4a and b suggests that the molecules were highly restrained and densely packed in the γ-phase. The planar fluorenone groups were aligned in the same direction, and all of the phenyl groups were also aligned parallelly. Hence, the γ-phase of the DPFO crystal contains strong face-to-face π···π aromatic interactions,[27] which promotes the formation of long-wavelength absorption and emission.[28,29] This is in significant contrast to the structure of the α-phase. In the α-phase, both the phenyl and fluorenone groups are perpendicular or formed a certain angle with their neighbors owing to CH···π interaction. Before the phase transition,

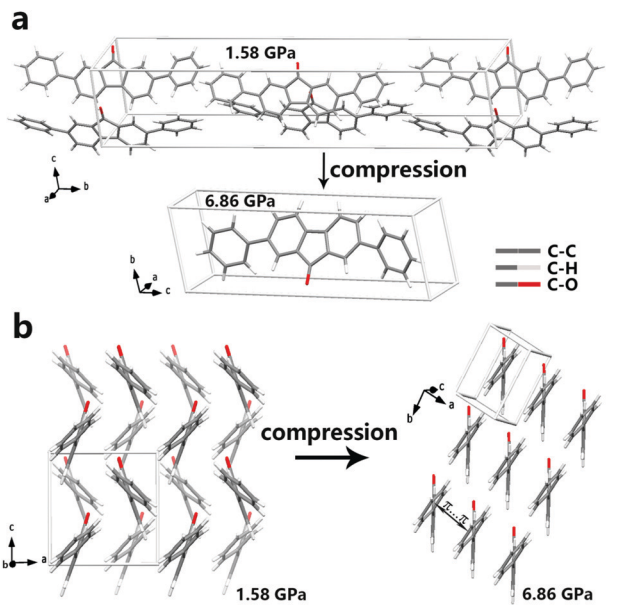

Fig. 4 (a) The evolution of the unit cell under compression. (b) The evolution of molecular packing under compression (the molecules in dark colour are closer to the viewer).

the dihedral angle (inset in Fig. 3b) between the phenyl group and the fluorenone group decreased and resulted in a better molecular co-planarity, which was responsible for the redshift of the emission and absorption spectra with a slow rate. After the phase transition, all of the DPFO molecules adopted face-to-face stacking, which was more energy favorable under high pressure due to the decrease in the volume. This stacking mode led to significant π···π overlapping and made the DPFO reveal large-scale redshift in the UV-vis absorption and PL spectra. With increasing pressure, the averaged single molecular volume of the γ-phase decreased (Fig. 3b), which indicated that the π···π distance between the neighboring phenyl unit (indicated in Fig. 4b) was reduced. The distance at 13.40 GPa was about 3.2 Å, which is much smaller than that of π···π interaction under ambient pressure in the range of 3.3–3.7 Å.[30] The decrease in the π···π distance was responsible for the continuous redshift after the phase transition. The increasing π···π interaction during compression was also evidenced by the resistance variation of DPFO (Fig. S5, ESI†), which gradually decreased with increasing pressure.[31]

Theoretical studies

To understand the large-scale redshift of the optical spectra under high pressure, the UV-vis absorption spectra for the selected aggregates of the α-phase and γ-phase were simulated by the Time-Dependent Density Functional Theory (TD-DFT) method.[32,33] The selected aggregates of the α-phase and γ-phase included four DPFO molecules, which represent the interactions between the neighboring molecules at 1.58 GPa and 6.86 GPa (see Fig. S6, ESI,† for the stacking patterns), respectively. As shown in Fig. 5a, the simulated UV-vis absorption spectra for 1.58 and 6.86 GPa exhibited strong-intensity peaks at 503 and 631 nm for the α- and γ-phase, respectively. This simulation is in good agreement with the longest wavelength absorption peaks of the experimental values (at around 495 and 660 nm under 1.30 and 6.50 GPa in the inset of Fig. 5a). The small discrepancies between the simulated and measured results might arise from the neglect of further molecular interactions due to the computational method and the limited simulation models.[34–36] More specifically, the strong peak of 503 nm at 1.58 GPa, which is attributed to the electronic state S4 of the α-phase, corresponds to the transition from the second molecular orbital below the highest occupied molecular orbital (HOMO−2) to the lowest unoccupied molecular orbital (LUMO). The two other weak peaks at 520 and 567 nm at 1.58 GPa correspond to the S3 and S1 states, respectively. On the other hand, the strong peak of 631 nm at 6.86 GPa is from the S1 state in the γ-phase, which is attributed to the transition from HOMO to LUMO. The additional peaks at 554, 516, 493 and 462 nm at 6.86 GPa correspond to S2, S3, S4 and S5, respectively (see Table 1 for the transition details of each electronic state). As shown in Fig. 5b and Fig. S7 (ESI†), there is less overlap of the wave-function between the neighboring DPFO molecules in the α-phase because of the CH···π repulsion. While in the

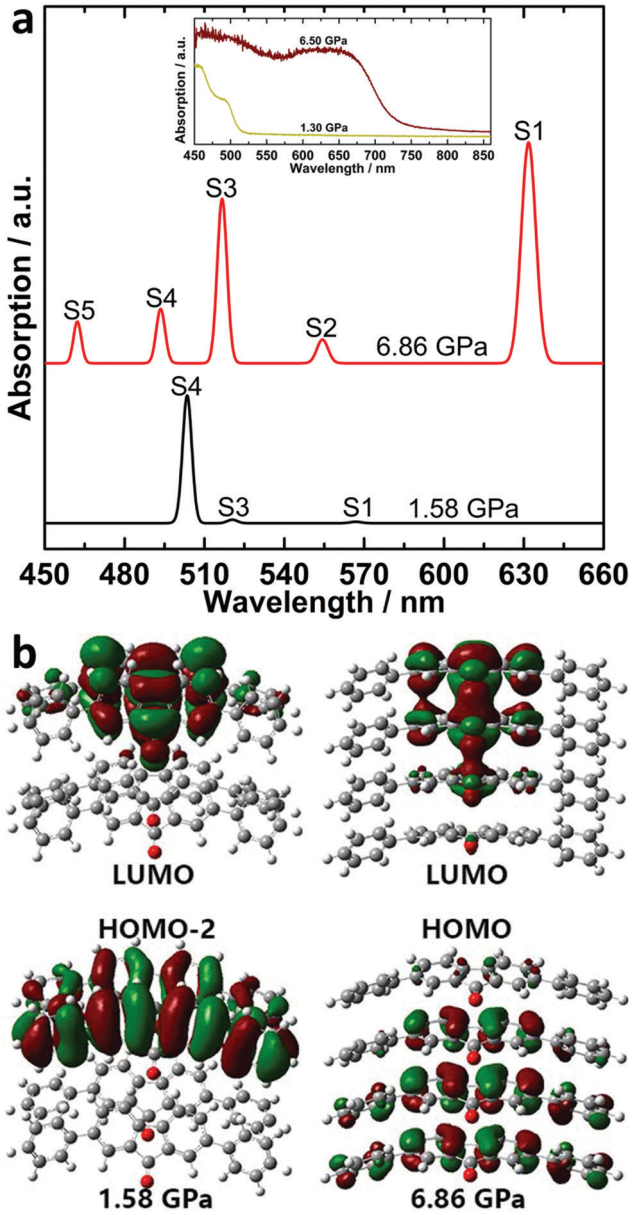

Fig. 5 (a) The TDDFT-calculated absorption spectra for the aggregates containing four molecules (inset: the corresponding experimental results of absorption) and (b) molecular orbitals contributing to the $S_0 \rightarrow S_3$ transition of DPFO at 1.58 GPa and to the $S_0 \rightarrow S_1$ transition of DPFO at 6.86 GPa.

γ-phase, the significant overlap of the wave-function between the neighboring molecules implies strong π···π intermolecular interactions, which leads to the decrease in the energy gap between the HOMO and LUMO for the γ-phase compared with the gap between the HOMO−2 and LUMO for the α-phase. Consequently, the high-density packing of the γ-phase enhances intermolecular interactions between the excited molecules and unexcited adjacent molecules. The smaller excitation energy of the electron promotion for the γ-phase makes great contribution to the longer-wavelength absorption and emission in DPFO after the phase transition.

Table 1 Time-dependent density functional theory (TDDFT) results for the five lowest-lying excited singlet states for diphenylfluorenone (DPFO) in the α-phase and γ-phase

State	Excitation energy (EE) (eV)	Oscillator strengths (OS)	Dominant orbital transitions contributions (DOTC)
α-Phase (1.58 GPa)			
S1	2.1870	0.0002	H−1 → L (51.4%), H → L (44.6%)[a]
S2	2.2964	0.0000	H → L (49.4%), H−1 → L (44.1%)
S3	2.3821	0.0005	H−1 → L+1(50.5%), H → L+1(45.0%)
S4	2.4624	0.0183	H−2 → L (66.4%)
S5	2.4815	0.0001	H → L+1 (48.4%), H−1 → L+1 (44.4%)
γ-Phase (6.86 GPa)			
S1	1.9624	0.0317	H → L (67.4%)
S2	2.2366	0.0034	H → L+1 (58.9%), H−1 → L (36.2%)
S3	2.3998	0.0236	H−1 → L (56.6%), H → L+1 (34.8%)
S4	2.5121	0.0078	H → L+2 (58.8%), H−1 → L+1 (33.9%)
S5	2.6822	0.0060	H−1 → L+1 (45.0%), H−2 → L (36.8%), H → L+2 (35.0%)

[a] H and L represent the highest occupied molecular orbital (HOMO) and lowest unoccupied molecular orbital (LUMO), respectively.

Conclusion

A reversible, tremendous, and continuous modulation of the absorption and luminescence spectra was realized by compressing DPFO crystals up to 13 GPa. Particularly, the photoluminescence spectra shifted from greenish-yellow (575 nm) to the near-IR region (875 nm), across the whole visible light region. By monitoring the evolutions of the IR spectra and the synchrotron XRD patterns under high pressure, we found that the α- to γ-phase transition was responsible for this drastic redshift. Compared with C–H···π interaction in the α-phase, the much denser stacking mode with the face-to-face conformations of the DPFO molecules in the γ-phase was energy-favored under high pressure. The TD-DFT calculation results further showed that the enhanced intermolecular π···π interaction in the γ-phase led to a decrease in the energy gap between the HOMO and LUMO and thus, resulted in the jump of the absorption and luminescence spectra. Our results indicate that DPFO may have a potential application in the molecular switch of modulating photoluminescence under high pressure. By measuring the crystal structure evolutions under different pressures, we found strong evidence that the π···π overlapping degree and π···π distance have a close relationship with the optical properties. This provides valuable insight into the construction and development of multi-colour luminescent materials.

Experimental

Sample preparation and high-pressure generation

DPFO was synthesized by a Suzuki coupling reaction and purified by a chromatography method following the literature procedures.[23] The sample was recrystallized in *n*-heptane three times and dried under vacuum before being used for the high-pressure experiments. The purity was confirmed by ^{1}H nuclear magnetic resonance (NMR), ^{13}C NMR and mass spectroscopy (MS) results. The crystal structure of DPFO at ambient pressure was confirmed by single-crystal XRD, which shows that it is in an orthorhombic phase with the $Ccm2_1$ space group.[23] Single crystals were selected and ground to a powder sample with a grain size of a few micrometres in an agate mortar for the high-pressure experiments. For the optical images, the single-crystal sample was used. A symmetric diamond anvil cell (DAC) with an anvil culet size of 300 μm in diameter was adopted for *in situ* high-pressure IR and photoluminescence spectra, as well as synchrotron XRD experiments. Type-IIa diamond anvils were used for the IR experiments to avoid absorption bands at 1000–1300 cm^{-1}. The T301 stainless steel gaskets were pre-compressed to 40 μm in thickness and center holes with d = 110 μm were drilled to serve as the sample chamber. The ruby fluorescence was used for pressure calibration in all the *in situ* high-pressure experiments.[37] All experiments were carried out at room temperature.

Optical measurements

The optical images of the evolution of the single-crystal DPFO under high pressure were gathered using a LEICA M205C microscope with silicone oil as the pressure-transmitting medium. The *in situ* high-pressure UV-vis absorption spectra were detected with a deuterium–halogen light source of 78 VA. Silicone oil was used as the pressure-transition medium. The background was calibrated by measuring the absorption without the sample at every pressure point. The *in situ* high-pressure photoluminescence spectra were measured by a Renishaw Raman microscope (RM1000) with a 488 nm excitation laser. High-pressure *in situ* IR experiments were carried out on a Bruker VERTEX 70v with a HYPERION 2000 microscope. A Globar was used as a conventional source. A 20 × 20 μm^2 aperture was used to collect the spectra in transmission mode in the range of 600–4000 cm^{-1} with a resolution of 2 cm^{-1}. The background of the IR measurements was collected from the diamond anvil absorption in the same aperture area.

XRD measurements

The *in situ* high-pressure synchrotron XRD data was measured at the 5A-MS-XRS beamline facility of the Pohang Accelerator Laboratory. Neon was loaded as the pressure-transmitting medium by a gas loading system. The XRD data were collected by a Mar345 detector, which was calibrated by the CeO_2 standard sample. The focused monochromatic X-ray beam wavelength was 0.69265 Å. The Dioptas program was used for

the preliminary data reduction of the XRD patterns.[38] The Rietveld refinement of the XRD data was conducted using the Jana 2006 program.[39]

Electrical resistance measurements

The resistance measurements were performed on an electrochemical impedance system with a combination of a Solartron 1260 impedance analyser and Solartron 1296 dielectric interface. A symmetric DAC fitted with diamonds with a d_{culet} = 500 μm was applied in a two-probe setting.[40] The steel supported cubic boron nitride gaskets and a Pt foil electrode were used for the measurements. The gaskets were pre-compressed to a thickness of 75 μm and a hole with d = 350 μm was drilled in the center to serve as the sample chamber. No pressure-transmitting medium was used for this measurement. AC voltage (100 mV) was applied in the frequency range between 0.01 Hz and 32 MHz. The experimental data were fitted and analyzed using Z-view software.

Computation details

For the calculation of the IR spectrum of DPFO, our DFT calculations were performed within the local density approximation[41] (LDA) implemented in the CASTEP[42] module of Material Studio. The IR parameters were calculated using the norm-conserving pseudopotentials with an energy cut-off for the plane wave basis set at 750 eV and k-points sampling less than $0.03 \times 2\pi$ A^{-1}.[43] To analyze the UV-vis spectra of the DPFO system, TD-DFT as implemented in Gaussian 09 D01[44] was performed with the B3LYP functional[45,46] and the 6-311G* basis set.[47] To obtain the simulated UV-vis absorption spectra, the excitations of the first five excited states were taken into consideration. The molecular aggregates containing four DPFO molecules were selected for the α-phase and γ-phase. To compare with the experimental UV-vis absorption spectra, the corresponding stacking styles of the two different phases were kept fixed, where the four molecules were arranged in a herringbone stacking pattern facilitating C–H$\cdots\pi$ interactions of the α-phase and in a linear accumulation pattern emphasizing the $\pi\cdots\pi$ stacking interactions of the γ-phase.

Conflicts of interest

There are no conflicts to declare.

Acknowledgements

The authors acknowledge the support of the National Natural Science Foundation of China (NSFC, Grant No. 21601007, 21773168, 21771011, and 21875006). The authors also acknowledge the support from the Top 1000-Talents Award and "the Fundamental Research Funds for the Central Universities", Nankai Universities (Grant No. 63196009). The calculation work was supported by the NSFC (Grant No. 11704024 and 21803033) and the Yong Elite Scientists Sponsorship Program by Tianjin (No. TJSQNTJ-2018-18). The authors acknowledge Dr. Dongzhou Zhang for his help on the XRD measurements at the GeoSoilEnviroCARS (The University of Chicago, Sector 13), Advanced Photon Source (APS), Argonne National Laboratory. The GeoSoilEnviroCARS is supported by the National Science Foundation – Earth Sciences (EAR – 1634415) and the Department of Energy – GeoSciences (DE-FG02-94ER14466).

Notes and references

1 D. Yan and D. G. Evans, *Mater. Horiz.*, 2014, **1**, 46–57.
2 Z. G. Chi, X. Q. Zhang, B. J. Xu, X. Zhou, C. P. Ma, Y. Zhang, S. W. Liu and J. R. Xu, *Chem. Soc. Rev.*, 2012, **41**, 3878–3896.
3 K. Nagura, S. Saito, H. Yusa, H. Yamawaki, H. Fujihisa, H. Sato, Y. Shimoikeda and S. Yamaguchi, *J. Am. Chem. Soc.*, 2013, **135**, 10322–10325.
4 K. S. Yook and J. Y. Lee, *Adv. Mater.*, 2014, **26**, 4218–4233.
5 B. Zhou and D. Yan, *Adv. Funct. Mater.*, 2019, **29**, 1807599.
6 Y. Yan and Y. S. Zhao, *Chem. Soc. Rev.*, 2014, **43**, 4325–4340.
7 J. Xu, S. Semin, T. Rasing and A. E. Rowan, *Small*, 2015, **11**, 1113–1129.
8 Q. Kong, Q. Liao, Z. Xu, X. Wang, J. Yao and H. Fu, *J. Am. Chem. Soc.*, 2014, **136**, 2382–2388.
9 J. Xu, S. Semin, J. Cremers, L. Wang, M. Savoini, E. Fron, E. Coutino, T. Chervy, C. Wang, Y. Li, H. Liu, Y. Li, P. Tinnemans, P. H. J. Kouwer, T. W. Ebbesen, J. Hofkens, D. Beljonne, A. E. Rowan and T. Rasing, *Adv. Opt. Mater.*, 2015, **3**, 948–956.
10 X. Li, S. Semin, L. A. Estrada, C. Yuan, Y. Duan, J. Cremers, P. Tinnemans, P. Kouwer, A. E. Rowan, T. Rasing and J. Xu, *Chin. Chem. Lett.*, 2018, **29**, 297–300.
11 H. Lin, X. Chang, D. Yan, W.-H. Fanga and G. Cui, *Chem. Sci.*, 2017, **8**, 2086–2090.
12 D. Yan, H. Yang, Q. Meng, H. Lin and M. Wei, *Adv. Funct. Mater.*, 2014, **24**, 587–594.
13 Y. Yan, C. Zhang, J. Yao and Y. S. Zhao, *Adv. Mater.*, 2013, **25**, 3627–3638.
14 Z.-Q. Yao, J. Xu, B. Zou, Z. Hu, K. Wang, Y.-J. Yuan, Y.-P. Chen, R. Feng, J.-B. Xiong, J. Hao and X.-H. Bu, *Angew. Chem., Int. Ed.*, 2019, **58**, 5614–5618.
15 Y. Wang, X. Lu, W. Yang, T. Wen, L. Yang, X. Ren, L. Wang, Z. Lin and Y. Zhao, *J. Am. Chem. Soc.*, 2015, **137**, 11144–11149.
16 B. Lu, Y. Zhang, X. Yang, K. Wang, B. Zou and D. Yan, *J. Mater. Chem. C*, 2018, **6**, 9660–9666.
17 Y. Liu, Q. Zeng, B. Zou, Y. Liu, B. Xu and W. Tian, *Angew. Chem., Int. Ed.*, 2018, **57**, 15670–15674.
18 H. Yuan, K. Wang, K. Yang, B. Liu and B. Zou, *J. Phys. Chem. Lett.*, 2014, **5**, 2968–2973.
19 Y. Dong, B. Xu, J. Zhang, X. Tan, L. Wang, J. Chen, H. Lv, S. Wen, B. Li, L. Ye, B. Zou and W. Tian, *Angew. Chem., Int. Ed.*, 2012, **51**, 10782–10785.
20 Y. Wang, X. Tan, Y.-M. Zhang, S. Zhu, I. Zhang, B. Yu, K. Wang, B. Yang, M. Li, B. Zou and S. X.-A. Zhang, *J. Am. Chem. Soc.*, 2015, **137**, 931–939.
21 Z. Ma, X. Meng, Y. Ji, A. Li, G. Qi, W. Xu, B. Zou, Y. Ma, G.-C. Kuang and X. Jia, *Dyes Pigm.*, 2019, **162**, 136–144.
22 Y. Gu, K. Wang, Y. Dai, G. Xiao, Y. Ma, Y. Qiao and B. Zou, *J. Phys. Chem. Lett.*, 2017, **8**, 4191–4196.

23 J. Xu, S. Semin, D. Niedzialek, P. H. J. Kouwer, E. Fron, E. Coutino, M. Savoini, Y. Li, J. Hofkens, H. Uji-I, D. Beljonne, T. Rasing and A. E. Rowan, *Adv. Mater.*, 2013, **25**, 2084–2089.
24 M. Savoini, L. Huber, H. Cuppen, E. Abreu, M. Kubli, M. J. Neugebauer, Y. Duan, P. Beaud, J. Xu, T. Rasing and S. L. Johnson, *ACS Photonics*, 2018, **5**, 671–677.
25 Y. Duan, C. Ju, G. Yang, E. Fron, E. Coutino-Gonzalez, S. Semin, C. Fan, R. S. Balok, J. Cremers, P. Tinnemans, Y. Feng, Y. Li, J. Hofkens, A. E. Rowan, T. Rasing and J. Xu, *Adv. Funct. Mater.*, 2016, **26**, 8968–8977.
26 C. Dong, *J. Appl. Crystallogr.*, 1999, **32**, 838.
27 M. L. Glowka, D. Martynowski and K. Kozlowska, *J. Mol. Struct.*, 1999, **474**, 81–89.
28 J. D. Wuest, *Nat. Chem.*, 2012, **4**, 74–75.
29 D. Yan, A. Delori, G. O. Lloyd, T. Friscic, G. M. Day, W. Jones, J. Lu, M. Wei, D. G. Evans and X. Duan, *Angew. Chem., Int. Ed.*, 2011, **50**, 12483–12486.
30 H.-F. Chen, W.-Y. Hung, S.-W. Chen, T.-C. Wang, S.-W. Lin, S.-H. Chou, C.-T. Liao, H.-C. Su, H.-A. Pan, P.-T. Chou, Y.-H. Liu and K.-T. Wong, *Inorg. Chem.*, 2012, **51**, 12114–12121.
31 L.-H. Xie, Q.-D. Ling, X.-Y. Hou and W. Huang, *J. Am. Chem. Soc.*, 2008, **130**, 2120–2121.
32 H. H. Heinze, A. Görling and N. Rösch, *J. Chem. Phys.*, 2000, **113**, 2088–2099.
33 R. E. Stratmann, G. E. Scuseria and M. J. Frisch, *J. Chem. Phys.*, 1998, **109**, 8218–8335.
34 H. Zhang, X. Zheng, N. Xie, Z. He, J. Liu, N. L. C. Leung, Y. Niu, X. Huang, K. S. Wong, R. T. K. Kwok, H. H. Y. Sung, I. D. Williams, A. Qin, J. W. Y. Lam and B. Z. Tang, *J. Am. Chem. Soc.*, 2017, **139**, 16264–16272.
35 J. Wang, X. Gu, P. Zhang, X. Huang, X. Zheng, M. Chen, H. Feng, R. T. K. Kwok, J. W. Y. Lam and B. Z. Tang, *J. Am. Chem. Soc.*, 2017, **139**, 16974–16979.
36 A. Bandyopadhyay, D. Ghosh and S. K. Pati, *J. Phys. Chem. Lett.*, 2018, **9**, 1605–1612.
37 H. K. Mao, J. Xu and P. M. Bell, *J. Geophys. Res.*, 1986, **91**, 4673–4676.
38 C. Prescher and V. B. Prakapenka, *High Pressure Res.*, 2015, **35**, 223–230.
39 V. Petricek, M. Dusek and L. Palatinus, *Z. Kristallogr.*, 2014, **229**, 345–352.
40 M. Yue, Y. Wang, L. Wang, X. Lin, K. Li, H. Zheng and T. Yang, *Chin. Chem. Lett.*, 2018, **29**, 328–330.
41 J. P. Perdew and A. Zunger, *Phys. Rev. B: Condens. Matter Mater. Phys.*, 1981, **23**, 5048–5079.
42 S. J. Clark, M. D. Segall, C. J. Pickard, P. J. Hasnip, M. J. Probert, K. Refson and M. C. Payne, *Z. Kristallogr.*, 2005, **220**, 567–570.
43 S. Baroni, S. de Gironcoli, A. dal Corso and P. Giannozzi, *Rev. Mod. Phys.*, 2001, **73**, 515–562.
44 M. J. Frisch, G. W. Trucks, H. B. Schlegel, G. E. Scuseria, M. A. Robb, J. R. Cheeseman, G. Scalmani, V. Barone, B. Mennucci, G. A. Petersson, *et al.*, *Gaussian 09, revision D.01*, Gaussian, Inc., Wallingford, CT, 2010.
45 C. Lee, W. Yang and R. G. Parr, *Phys. Rev. B: Condens. Matter Mater. Phys.*, 1988, **37**, 78.
46 P. Stephens, F. Devlin, C. Chabalowski and M. J. Frisch, *J. Phys. Chem.*, 1994, **98**, 11623–11627.
47 X. Gong, H. Xiao and B. V. D. Graff, *THEOCHEM*, 1997, **393**, 207.